Article

Activity-dependent glassy cell mechanics Ⅰ:

Mechanical properties measured with active microrheology

K. Umeda, 1 K. Nishizawa, 2 W. Nagao, 1 T. Miyamoto, 3,4 H. Ebata, 1 and *D. Mizuno 1

1. Department of Physics, Kyushu University, 819-0395 Fukuoka, Japan.
2. Institute of Developmental Biology of Marseille, Campus de Luminy case 907, 13288 Marseille Cedex 09, France.
3. Department of Endocrinology and Metabolism, Faculty of Medicine, University of Tsukuba, 1-1-1 Tennodai, Tsukuba, Ibaraki 305-8575, Japan
4. Transborder Medical Research Center, University of Tsukuba, Ibaraki, Japan.

* Correspondence: mizuno@phys.kyushu-u.ac.jp; Tel.: +81-92-802-4092

Received: date; Accepted: date; Published: date

running title：Critical jamming of living cytoplasm

Abstract: The active microrheology was conducted in living cells by applying optical-trapping force to vigorously-fluctuating tracer beads with the feedback-tracking technology. Complex shear viscoelastic modulus $G(\omega) = G'(\omega) - iG''(\omega)$ was measured in HeLa cells in an epithelial-like confluent monolayer. We found that $G(\omega) \propto (-i\omega)^{0.5}$ in large range of frequencies (0.1 Hz < $\omega/2\pi$ <10 kHz). Actin disruption and cell-cycle progression from G1 to S, G2 phases only limitedly altered $G(\omega)$ in living cells. On the other hand, $G(\omega)$ was dependent on cell metabolism; the ATP-depleted cells increased elastic modulus $G'(\omega)$ at low frequencies by giving rise to a constant plateau as $G(\omega) = G_0 + A(-i\omega)^{0.5}$. Both the plateau and the additional frequency dependency proportional to $(-i\omega)^{0.5}$ of ATP-depleted cells are consistent to the typical rheological response of colloidal jamming. On the other hand, the plateau G_0 disappeared in the ordinary metabolically active cells, implying that the living cells fluidize their internal states towards critical jamming point.

Statement of Significance: Intracellular mechanical properties were measured using the optical-trap-based microrheology. Despite the common expectations, shear viscoelasticities were hardly concerned with reorganization of cytoskeletal structures during cell-cycle progressions, nor with the artificial disruption of actin cytoskeletons induced with chemical inhibitors. Rather, the mechanics of cell interiors were governed by the glassy cytoplasm. Rubber-like elasticities in solidified ATP-depleted cells disappeared in living cells with ordinary metabolic activities, indicating the activity-dependent fluidization. Instead of the complete fluidic response, however, we observed the characteristic power-law viscoelasticities $G(\omega) \propto (i\omega)^{0.5}$ in the whole range of frequencies observed. Based on the recent understanding of jamming rheology, we discuss that cells fluidize their internal state towards the critical jamming transition.

Keywords: cell mechanics; microrheology; active fluidization; glassy cytoplasm; cell cycle; cytoskeleton

INTRODUCTION

Intracellular mechanics are fundamental for biology because they govern the dynamics of physiological processes which are performed by functional bio-macromolecules (1-3). For instance, motor proteins and other mechanoenzymes play their own roles by utilizing the energy derived from metabolism (4-6). Since they need to change their shapes to catalyze biochemical reactions (7, 8) and need to be transported to appropriate locations at relevant occasions (9), their performance depends on the mechanical properties (*i.e.*, fluidity) of surrounding medium. At the same time, cells also need mechanical stabilities in order to maintain their complex internal organizations. Living cells thus meet these apparently conflicting requirements: dynamic fluidity and mechanical stability. However, the physical machinery and principles underlying the complex intracellular mechanics are mostly elusive (10, 11). It has been believed that mechanics of cells are largely determined by the cytoskeletal organization (12, 13). On the other hand, other colloidal bio-macromolecular constituents also remarkably contribute to mechanics because they are densely packed in cells (14, 15) and bring the intracellular environments into glassy state (3, 16-18). As one of typical soft materials, mechanical properties of these biological materials (cytoskeletons and colloidal bio-macromolecules) are profoundly regulated when they are driven out of equilibrium. For instance, *in vitro* experiments have shown that cytoskeletons stiffen (19-24) and glassy colloids fluidize (25, 26) when they are subjected to the shear stress, locally applied forces and other mechanical loads. In living cells, mechanical loads may be imposed by the metabolic activity of mechanoenzymes. Nevertheless, how these factors, *i.e.*, cytoskeletons, cytoplasm, their organizations, and metabolic activity, are integrated in the intracellular mechanics is poorly understood.

Microrheology (MR) is a method to investigate the viscoelastic properties of a medium at microscopic (~ μm) length scales (27), by tracking the motion of micron-sized tracer beads imbedded in a specimen (28, 29). In active microrheology (AMR) (30, 31), an external force is applied to a tracer bead, and its response displacements are measured. When a sinusoidal force is applied to the bead, we obtain the complex shear viscoelastic modulus $G(\omega) = G'(\omega) - iG''(\omega)$ of surrounding medium as a function of the angular frequency ω. Here, G' and G'' are the real and imaginary part of the complex modulus $G(\omega)$. AMR can be performed simultaneously by applying the optical-trapping force to the probe particle, and by measuring the probe displacements with the back-focal-plane laser interferometry technique (BFPI) (31, 32). Because of the vigorous non-thermal fluctuations, however, a probe particle in living cells moves out of the laser focus within the experimental periods of time. Although a strong laser could trap the probe in the laser focus, it also hinders the bead motion. It then causes large errors in estimating the intrinsic response and the fluctuation that should have occurred if the optical trapping was not performed. In our prior study, we therefore developed an optical-trap-based MR implemented with three-dimensional feedback-controlled sample stage (feedback-tracking MR, see supplementary S1) (10, 33). This technique allowed us to stably track a vigorously-fluctuating probe particle in living cells with the laser power as small as 0.5 mW, which was remarkably decreased compared

to ordinary optical-trapping measurements (31, 34). As seen in Fig. S2, this non-invasive technology is crucial to conduct optical-trap-based MR in living cells.

Using this MR technique, we investigated the intracellular mechanics of living HeLa cells derived from cervical cancer while controlling their cell cycle, cytoskeletal organization, and metabolic activities. It is known that living cells dynamically change their internal organization during their cell-cycle progression. They replicate chromosomes, double the cytoplasmic components and reconstruct cytoskeleton structures (35). These processes are inherently mechanical since they proceed in conjunction with the force-related signaling cascades (36), as demonstrated in numbers of prior studies (36-38). Accordingly, it has been reported that elastic and viscous moduli of cells depend on the cell-cycle phase (39, 40). Note, however, that the techniques used in prior studies (AFM (13, 41), magnetic twisting cytometry (16, 42, 43), and micropipette aspiration) could probe mechanical properties of cell's "surfaces" at which actin cytoskeletons are densely expressed. Since cytoskeletons are less expressed in the middle of cells, it was not certain whether and how cell cycles and cytoskeletons affect the "intracellular" mechanics.

In HeLa cells, cultured in an epithelial-like monolayer sheet, we found that complex shear viscoelastic properties $G(\omega)$ showed a frequency dependence that was predicted for the disordered colloidal jamming $G(\omega) \propto (-i\omega)^{1/2}$ (10, 11). Dependency that was predicted and observed for cytoskeletons [$G(\omega) \propto (-i\omega)^{3/4}$ at large ω and $G(\omega) \propto (-i\omega)^{0}$ at small ω] (44, 45) was not observed. Besides, disruption of cytoskeletons hardly changed intracellular $G(\omega)$, clearly showing that intracellular mechanical properties are seldom affected by the expression of actin cytoskeletons. In order to examine the cell-cycle dependence, HeLa cells labelled with the fluorescent ubiquitination-based cell-cycle indicator (Fucci) were used (10). We found only small cell-cell differences in $G(\omega)$, and cytoplasmic mechanics of cells were altered merely marginally while they proceed from G1 phase to S/G2 phases.

After recognizing that intracellular mechanics are not strongly dependent on actin cytoskeletons and cell-cycle progression, we performed feedback-tracking MR in ATP-depleted HeLa cells (42). We found that the intracellular mechanical properties are highly dependent on the metabolic activities. The viscoelasticity increased in ATP-depleted HeLa cells. The plateau elasticity $G'(\omega) = G_0$ which is constant in frequencies appeared and dominated the modulus at low frequencies while $G(\omega) \propto (-i\omega)^{1/2}$ was still observed at larger ω, *i.e.*, $G(\omega) = G_0 + A(-i\omega)^{1/2}$. Our experimental results indicate that the mechanics of cell interior is mostly determined by the glassy cytoplasm (3, 11, 17). It is inferred that the mechanical energy supplied by the mechano-enzymes induced structural relaxations (10), and thus fluidized the cytoplasm (3, 11). The expected fluid-like response $G(\omega) \propto -i\omega\eta$ was not seen in our data likely because the frequency range was limited to 0.1 Hz or higher. Instead, our results imply that the rheological properties typical for the critical jamming state (46, 47) is achieved during the active fluidization of glassy cytoplasm (48).

124 **MATERIALS AND METHODS**

125 **Cell preparation**

126 HeLa cells and HeLa/Fucci2 cells (Riken, Cell Bank) were seeded on fibronectin-coated
127 glass-bottom petri dishes in Dulbecco's modified Eagle's medium (Wako, D-Mem, high
128 glucose) with glucose (1 mg/ml), penicillin (100 U/ml), streptomycin (0.1 mg/ml),
129 amphotericin B (250 mg/ml), and 10% fetal bovine serum (FBS) at 37°C. Cells were cultured
130 in the CO_2 incubator until they formed a confluent epithelial-like monolayer sheet. The probe
131 particles (melamine particles, 1 μm diameter, micro Particles GmbH) coated with
132 polyethylene glycol (PEG) strands (33) were introduced into the HeLa cells using a gene gun
133 (PDS-1000/He, Bio-Rad). PEG coating generally passivates probe surfaces; in aqueous
134 environments, hydrophilic PEG acts as a polymer brush and prevents sticking to other objects
135 or to other molecules. Excess beads that did not enter the cells were removed by washing the
136 dishes with phosphate-buffered saline. After replacing to the fresh medium, the dishes were
137 then placed in an CO_2 incubator for at least several hours until the cell damages were
138 recovered. Supplying CO_2 in the MR setup causes additional noise to the experimental data.
139 Therefore, MR experiments were performed in a CO_2-independent culture medium (Gibco,
140 L-15 medium) with 10% FBS serum. All measurements were performed at 37°C. For MR
141 experiments under ATP depletion and actin disruption, FBS was not included in the media
142 as written below.
143

144 **Actin disruption**

145 For disrupting actin network, polymerization of actin filaments were inhibited by adding
146 chemical agents (Cytochalasin D 50 μg/ml or Latrunculin B 10 μM). After MR experiments
147 were performed at 37°C in L-15 medium with 10% FBS (w/o chemical agents), culture
148 medium was replaced to that for actin disruption (Cytochalasin D or Latrunculin B, without
149 FBS). Cells were then incubated at 37 °C on the MR setup for ~30 min prior to the next MR
150 measurement so that actin network is disrupted in cells.
151

152 **ATP depletion**

153 High energy molecule ATP is mainly produced in cells via two metabolic pathways:
154 glycolytic in the cytoplasm and oxidative phosphorylation in mitochondria. Therefore, in
155 order to deplete intracellular ATP, cells were cultured in a nutrient free media with 50 mM
156 2-deoxy-D-glucose, 10 mM sodium azide (42, 49). 2-deoxy-D-glucose and sodium azide
157 inhibits glycolysis and oxidative ATP production, respectively.
158 HeLa cells were incubated in the medium for ATP depletion (L-15 medium with 50 mM
159 2-deoxy-D-glucose, 10 mM sodium azide, without FBS) at 37 °C for ~10 hours prior to the
160 MR measurements so that ATP stored in cells are consumed.

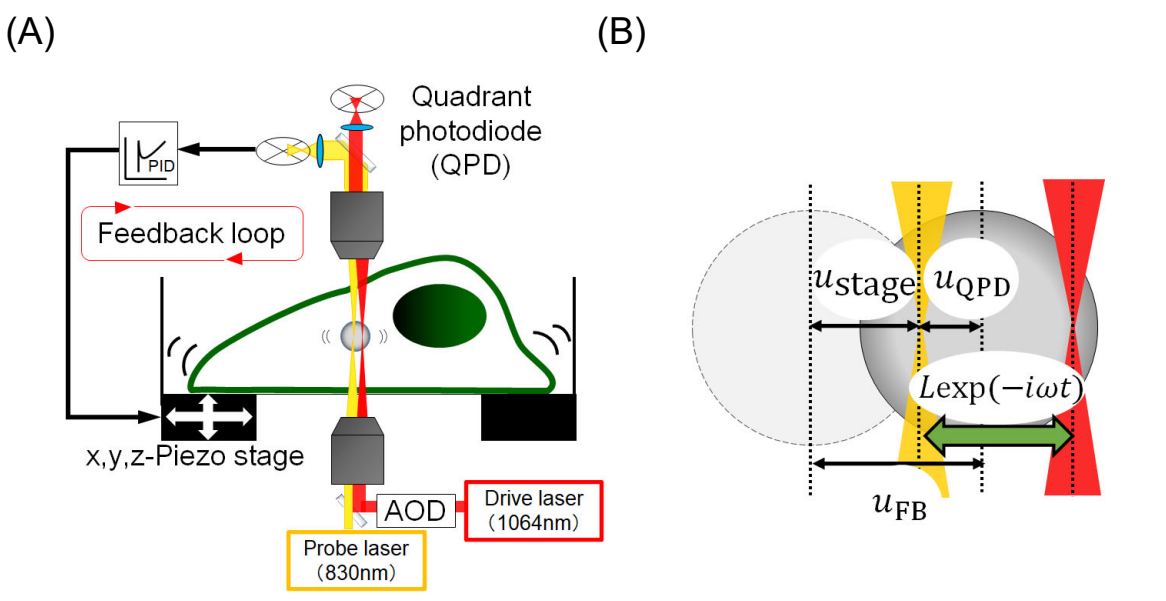

Fig. 1: (A) Schematic of the feedback-tracking microrheology setup. Fixed probe laser is used to measure u_{QPD} using quadrant photodiode (QPD). Drive laser is used for AMR to apply external force by oscillating with acousto-optic deflector (AOD). (B) Displacements of a probe $u(t)$ is obtained by the sum of the displacement of the piezo stage $u_{\mathrm{stage}}(t)$ and the displacement from the focus of the probe laser $u_{\mathrm{QPD}}(t)$. The focus of the drive laser is moved sinusoidally around the focus of the probe laser as $L\exp(-i\omega t)$

Luminescent ATP detection assay

Intracellular ATP was measured using a CellTiter-Glo® Luminescent Cell Viability Assay kit (Promega, G7570) according to the manufacturer's instructions. Briefly, 5,000 cells were plated on a 96-well plate and incubated for 24 h at 37°C in 5% CO_2. Following incubation, the medium was replaced with 50 µl of either: (1) control medium [phenol-red free DMEM (Thermo Fisher, 31053028) supplemented with 4 mM glutamine (Thermo Fisher, 25030081) and 1% Penicillin-Streptomycin Solution (Sigma-Aldrich, P4333)], or (2) control medium supplemented with 50 mM 2-deoxyglucose (Nacalai, 10722-11) and 10 mM NaN_3 (WAKO, 199-11095), and then incubated for 7 h at 37°C in 5% CO_2. Subsequently, 50 µl of reagent was directly added to the well and the contents were mixed for 2 min on an orbital shaker at 25°C. Luminescence was recorded after 30 min of incubation at 25°C in the dark.

AMR in living cells

The technical details for the conventional optical-trapping-based AMR (without feedback operation) were given elsewhere (31). We will repeat the essence here briefly for reader's convenience. As shown in Fig. 1A, a small sinusoidal force $F(t)=\hat{F}(\omega)e^{-i\omega t}$ was applied to a probe particle, by optically trapping it with the drive laser (λ =1064 nm Nd:YVO_4, Coherent Inc., Tokyo, Japan) whose focus position was controlled by the acousto-

optic deflector (AOD; DTSX-400-1064, AA Opto-Electronic, Orsay, France). The probe displacement synchronous to the applied force $u(t) = \hat{u}(\omega)e^{-i\omega t}$ was measured with the back-focal-plane laser interferometry (BFPI) conducted by the fixed probe laser ($\lambda = 830$ nm IQ1C140, Power Technology, Inc., Alexander, AR, USA) (32). The frequency response function $\tilde{\alpha}(\omega) = \alpha'(\omega) + i\alpha''(\omega) \equiv \langle \hat{u}(\omega) \rangle / \hat{F}(\omega)$ is then obtained as a complex quantity. The shear viscoelastic modulus $G(\omega)$ of the surrounding media is also obtained as a complex quantity via the Stokes relation extended to the sinusoidal response,

$$G(\omega) = 1/6\pi a\tilde{\alpha}(\omega). \quad (1)$$

where a is the radius of a spherical probe particle.

A tracer bead vigorously fluctuates in a living cell because the cytoplasm is driven far from equilibrium by the energy derived from metabolism. As explained in detail in Refs. (10, 33), such a fluctuating particle was smoothly tracked by the analog PID-feedback control of the piezo-mechanical sample stage on which the specimen was placed. The optical-trapping force was then stably applied to the probe particle by the oscillating drive laser while maintaining the probe particle in the focus of the fixed probe laser. As shown in Fig. 1B, the displacement of the probe particle from the probe laser u_{QPD}, which is measured by BFPI of the probe laser, is used to control the position of the piezo stage u_{stage} as

$$u_{\mathrm{stage}}(t) = \frac{1}{\tau}\int u_{\mathrm{QPD}}dt, \quad (2)$$

where τ (typically set at 10 ms ~ 100 ms) is the delay time for the feedback response of our experimental setup. The displacement u_{FB} of the probe in the coordinate system traveling with the feedback-controlled piezo stage is given as $u_{\mathrm{FB}} = u_{\mathrm{QPD}} + u_{\mathrm{stage}}$ (Fig. 1B). From Eq. (2), the frequency-response relation is obtained as,

$$\hat{u}_{\mathrm{FB}}(\omega) = (1 - i\omega\tau)\hat{u}_{\mathrm{stage}}(\omega) = \{1 - 1/(i\omega\tau)\}\hat{u}_{\mathrm{QPD}}(\omega), \quad (3)$$

where ^ denotes the amplitude of the sinusoidal signal, e.g. $u_{\mathrm{FB}}(t) = \hat{u}_{\mathrm{FB}}(\omega)\exp(-i\omega t)$. Eq. (3) denotes that $u_{\mathrm{QPD}}(t)$ and $u_{\mathrm{stage}}(t)$ are high- and low-pass filtered from the total probe displacement $u_{\mathrm{FB}}(t)$. Then, the slow/large displacements of the probe are tracked by piezo stage as u_{stage} whereas the fast/small displacements are measured with QPD as u_{QPD}. By measuring either $\hat{u}_{\mathrm{stage}}$ or $\hat{u}_{\mathrm{QPD}}$ as a function of frequencies, we obtain the total probe response $\hat{u}_{\mathrm{FB}}(\omega)$ under the feedback tracking. By estimating the sinusoidal force $\hat{F}_{\mathrm{FB}}(\omega)$ applied to the probe under the feedback (as given in the supplementary S1), we obtain the probe particle's response function as $\tilde{\alpha}(\omega) = \langle \hat{u}_{\mathrm{FB}}(\omega) \rangle / \hat{F}_{\mathrm{FB}}(\omega)$. We then obtain $G(\omega)$ via Eq. (1)

Statistical analysis

Since the distributions of *G'* and *G''* were non-Gaussian, statistical analysis was performed by using the Mann–Whitney U test, unless otherwise stated in the figure caption. *P* values < 0.05 were considered as significant difference. All the statistical tests were performed by Igor and Matlab software.

RESULTS

Marginal contribution of actin cytoskeletons to intracellular mechanics

Using the feedback-tracking AMR, we measured the shear viscoelastic modulus of HeLa cells derived from a cervical cancer. Melamine particles ($2a$ = 1 μm) were incorporated into cells forming the epithelial-like confluent monolayer on the surface of the glass-bottom dish. Particles incorporated at the center of cells between the cell membrane and the nuclear membrane were used as probes. The average of the complex shear modulus of the untreated HeLa cells is shown in Fig. 2 together with the standard deviation (n = 21). Filled circles in (A) and open triangles in (B) represent real (G') and imaginary (G'') part of the complex shear modulus, $G(\omega) = G'(\omega) - iG''(\omega)$. Curves show raw data before averaging. Markers are the averaged values and bars indicate the log-normal SD. Since the logarithms of mechanical properties are distributed approximately with Gaussian (42), averages and SDs were calculated for the logarithm of experimental results. Our results showed the characteristic frequency dependence in the form of $G(\omega) \propto (-i\omega)^{0.5}$. It has been reported that cytoskeletons prepared *in vitro* exhibit an elastic plateau $G(\omega) \propto (-i\omega)^{0}$ at low frequencies, and a power-law dependency in the form of $G(\omega) \propto (-i\omega)^{0.75}$ at higher frequencies (21, 22, 45). The frequency dependency, which is now accepted as the hallmark of cytoskeletons (24, 50), is explained by the theory for the semi-flexible polymer networks (44, 51, 52). For biological cells, $G(\omega)$ consistent to the expectation was found when MR

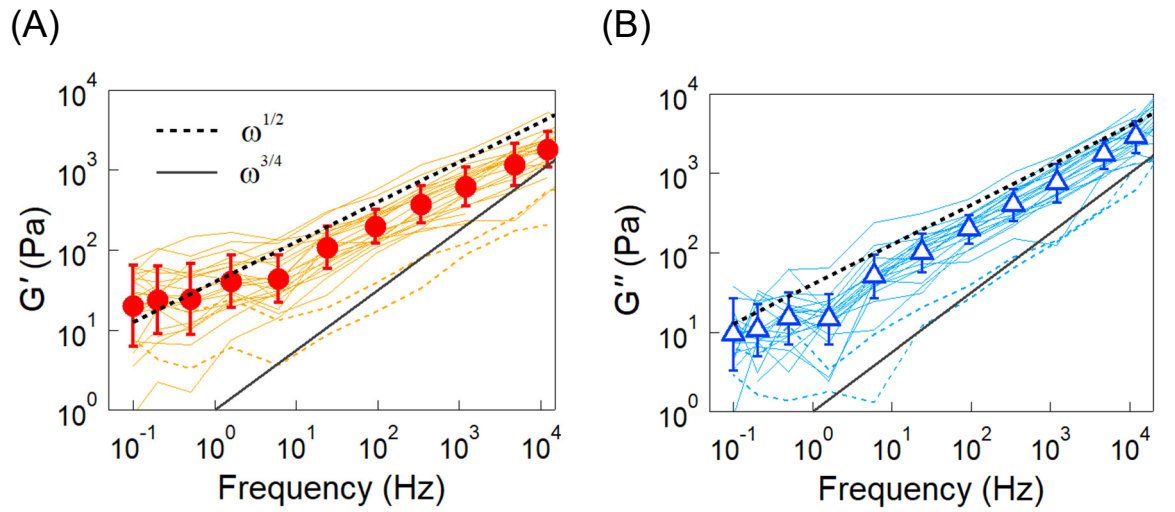

FIGURE 2 Intracellular shear viscoelasticities measured with AMR using $2a$ = 1 μm diameter melamine particles. (A) $G'(\omega)$ and (B) $G''(\omega)$ of HeLa cells in a confluent monolayer formed on glass substrate. Curves are the raw data obtained in 23 different cells. Data shown in broken curves were excluded from the average (n =21). Since cell cycles were not monitored, cells in different cell-cycle phases (G1, S, and G2) are included. Circles and triangles are the statistical average, and bars indicate the log-normal SD. Broken and solid lines show the power-law dependency typical for glassy cytoplasm ($\propto \omega^{0.5}$) and cytoskeletal networks ($\propto \omega^{0.75}$), respectively. The result follows $\propto \omega^{0.5}$ in a wide range of frequencies, indicating that the intracellular mechanics are predominantly governed by the glasssy cytoplasm.

was conducted using probe particles specifically coupled to actin cytoskeletons on cell surfaces (10, 53). On the other hand, the power-law dependence $G(\omega) \propto (-i\omega)^{0.5}$ observed in this study is not consistent to that expected for cytoskeletons. It is to be noted that the probe particles used in this study were coated with polyethylene glycol polymers that generally inhibit adherence to objects in cells including cytoskeletons. Besides, the probes were incorporated deep inside of living cells where actin cytoskeletons are only sparsely expressed.

In order to clarify the contribution of actin cytoskeletons to intracellular mechanics, we conducted AMR in HeLa cells in which actin cytoskeletons were disrupted. After conducting the first AMR experiments in untreated HeLa cells, actin polymerization was inhibited by adding Cytochalasin D or Latrunculin B to culture medium (54, 55). The second AMR measurements were then performed using the same particles as those used in the first AMR. Since $G(\omega)$ shows general trend proportinal to $(-i\omega)^{0.5}$, results normalized as $G'/\omega^{0.5}$ are shown in Fig. 3 in order to clarify the effect of the chemical dose at each frequency. Cytochalasin D at 50 μg/ml did not alter $G(\omega)$ in any frequency range (n = 9, Fig. 3A, and B). Statistical tests at each frequency were conducted for $G'(\omega)$ and $G''(\omega)$ before and after the addition of Cytochalasin D. P values obtained by the Mann–Whitney U test were larger than 0.05 for all the frequency of $G'(\omega)$ and $G''(\omega)$, which indicated no significant difference. Similar results were obtained by treating cells with another inhibitor for actin polymerization, Latrunculin B at 10 μM (Fig. S3). On the other hand, cells changed their morphology after the inhibitors were administrated (Fig. 3C). They became more rounded while leaving branched protrusions, lost cell-cell contact, and some cells are removed from the glass substrate. These observations indicate that the inhibitors worked effectively and disrupted cytoskeletal organizations since actin cytoskeletons are responsible for maintaining the shape of cells and their adhesion to the substrate. We thus conclude that actin cytoskeletons do not remarkably contribute to intracellular mechanical properties in epithelial cells cultured in confluent monolayer.

HeLa cells in confluent monolayers are laterally confined and polarized in the ordinary condition. They are roughly as tall as they are wide, and tightly connected to each other. In such epithelial-like tissue, actin stress fibers are densely expressed at the cell-cell and cell-substrate interfaces, and they contribute to the organizations of the tissue. The disruption of actin thus remarkably affects cell morphology. In prior studies, mechanical properties of cells have been measured by using techniques, *e.g.* AFM (atomic force microscopy)(13, 41, 56), MTC(16, 17) (magnetic twisting cytometry) *etc* (42, 57, 58). These techniques had shown that the mechanical properties of cells indeed depend on actin expression (59). It is therefore commonly believed that the mechanical properties of cells are directly correlated with their shape and cytoskeletal organizations (57, 58), in contrast to our experimental results. It is to be noted, however, that the techniques used in prior studies measure the properties of cell surfaces at which actin cytoskeletons are densely expressed. Considering that actins are less expressed inside of the epithelial cells in a confluent monolayer, results obtained in this study are reasonable and do not contradict to any of the prior measurements conducted on cell surfaces.

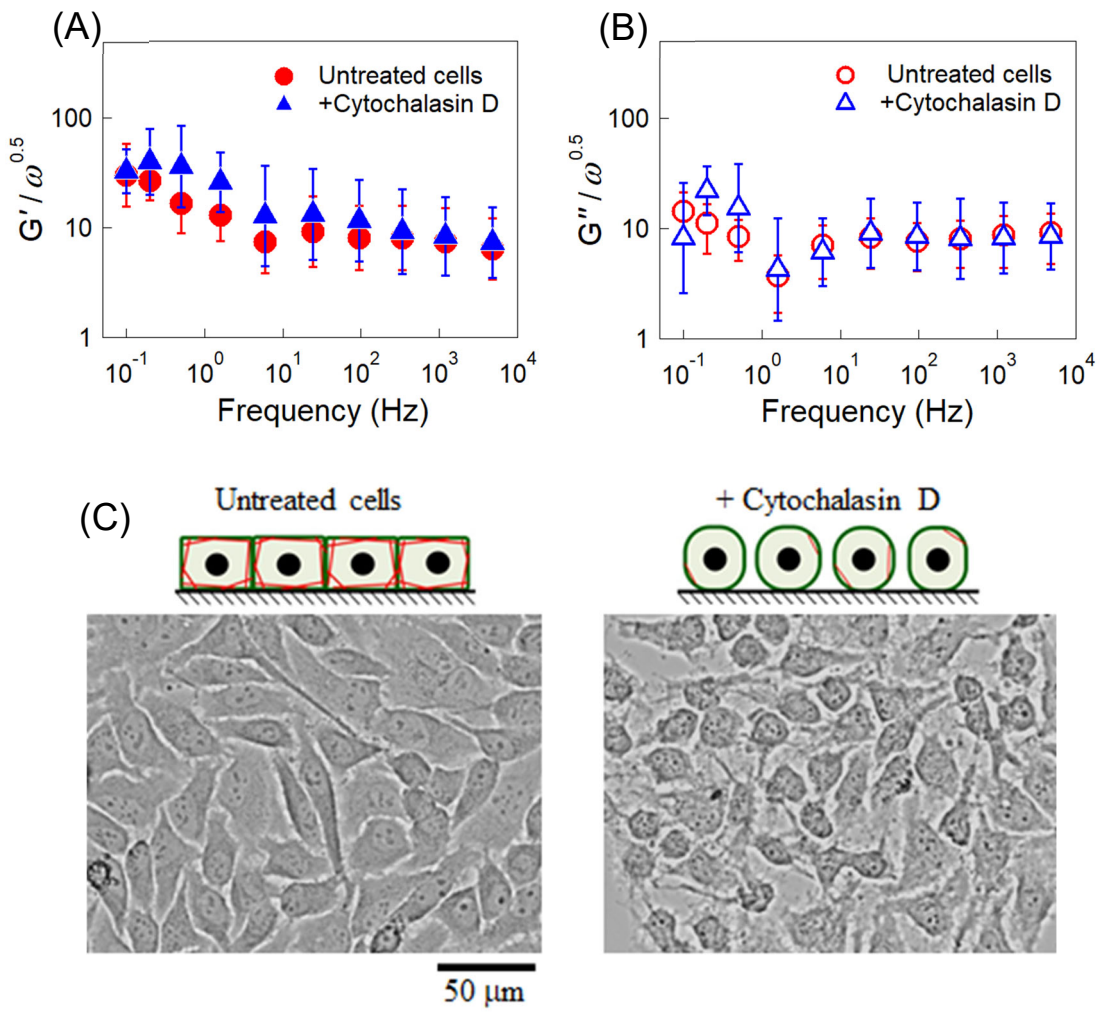

FIGURE 3 (A) $G'/\omega^{0.5}$ and (B) $G''/\omega^{0.5}$ of HeLa cells, untreated (circles) and treated (triangles) by 50 μg/ml Cytochalasin D. The same probe particles in the same cells were measured before and after adding Cytochalasin D to culture media (n = 9). Bars indicate the log-normal SD. The similar experiments performed before and after treated by 10 μM Latrunculin B are given in Fig. S3. (C) A microscopy image of HeLa cells. When actin cytoskeletons were disrupted with 50 μg/ml Cytochalasin D, cells have strongly contracted, leaving branched protrusions. (A, B) The Mann–Whitney U test was used to calculate the P value between untreated cells and cells treated by 50 μg/ml Cytochalasin D. No significant difference was observed for all the frequencies.

Cell surface elasticities measured using the conventional techniques were usually widely distributed by orders of magnitude (42, 43, 56). The organization of actin cytoskeleton at the cell cortex are heterogeneous and alter with time. Depending on the situations, actins bundle to thick fibers, couple to cell membranes, and create tensions by actomyosin contractile activities, leading to remarkable stiffening (21, 22, 60). All these and many other factors contribute to variate the mechanical properties of cell surfaces. On the other hand, $G(\omega)$ in living cytoplasm only narrowly distributes although they were measured with different probes in different cells. This observation also supports that the intracellular mechanics of epithelium are not strongly associated with cytoskeletons.

Cell mechanics during cell-cycle progression

Next, we performed feedback-tracking AMR in HeLa cells during their cell-cycle progression. HeLa cells used here (HeLa/Fucci2) were labelled with Fucci system that enables to identify G1 and S/G2 phases by the fluorescence color in the cell nucleus (61). The cell-cycle phases were then monitored with the fluorescence microscopy which were implemented in our MR experimental setup. In Fig. 4, we show the normalized shear viscoelastic modulus ($G'/\omega^{0.5}$ and $G''/\omega^{0.5}$) of HeLa cells as a function of frequency. Red and Green symbols indicate cells at G1 and S/G2 phases respectively. *G'* of S/G2 phase showed slight but significant increase for several frequencies, while *G''* exhibited significant difference at only 0.5 and 24 Hz.

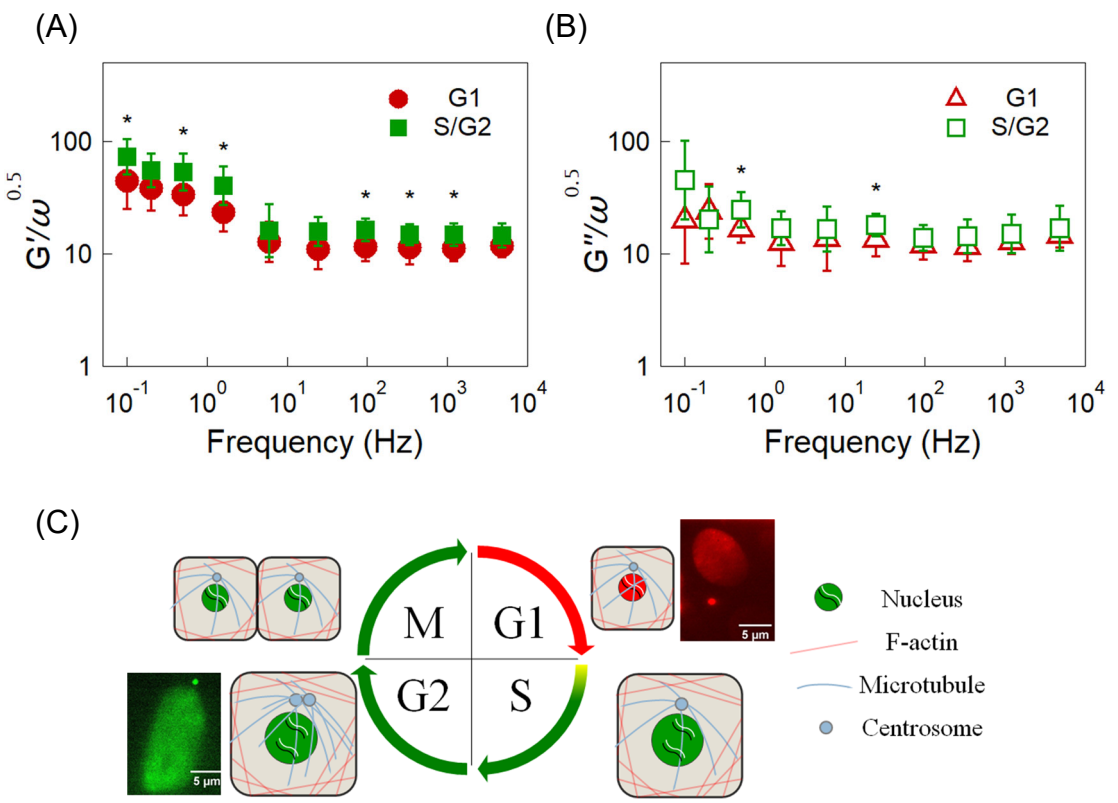

FIGURE 4 (A) $G'/\omega^{0.5}$ of HeLa/Fucci2 cells in G1 (circles, n = 12) and S/G2 phases (squares, n = 9). (B) $G''/\omega^{0.5}$ of HeLa/Fuuci2 cells in G1 (circles) and S/G2 phases (squares). Bars indicate the estimate of the log-normal SD. No remarkable differences were observed. (C) Schematic illustration of Fucci system used for identifying the cell-cycle phases. The Mann–Whitney U test was used to calculate the P value between G1 and S/G2 phases. *: $P < 0.05$. No symbol: $P > 0.05$.

As explained in the introduction, various processes that occur during cell-cycle progression is inherently mechanical. Especially, cells in M Phase may experience drastic variation in intracellular organization and could exhibit mechanical properties more largely different from other phases (58, 62, 63). However, AMR experiments were not conducted in M phase cells in this study because mitosis and cytokinesis are highly dynamic and complete in relatively short period of time. In the literature, the cell-cycle dependency of cell mechanics has been investigated with the atomic force microscopy (AFM) (39) and micropipette aspiration (40), both of which showed 50~100% increase of surface elasticity of S-Phase cells compared with that of G1-phase cells. In this study, the intracellular $G(\omega)$ in S/G2 phase slightly increased compared to cells at G1 phase; *G'* and *G''* of S/G2 phase were averagely 40 % and 30% larger than those of G1 phase, respectively. Here, we emphasize again that our results and prior studies do not contradict. Results are different because our intracellular $G(\omega)$ is indifferent to actin cytoskeletons, but the methodologies used in prior studies measure the cytoskeletons at the cell surfaces whose expression is likely strongly affected during the cell-cycle progressions.

ATP-dependent intracellular mechanical properties

After finding that the influence of cytoskeletons and cell-cycle phase on the intracellular mechanics is marginal, we now investigate the metabolism dependency of active mechanics in HeLa cells. In order to regulate the metabolic activity, cells were incubated with the culture media for ATP-depletion (42). Intracellular ATP was measured using the luminescent ATP detection assay. Figure 5A shows that the ATP level significantly decreased by more than a order of magnitude in ATP depleted cells. It was found that the ATP-depleted cells increased elastic plateau as $G(\omega) \propto G_0 + A(-i\omega)^{0.5}$ which is in contrast to $G(\omega) \propto (-i\omega)^{0.5}$ for untreated cells, as shown in Fig. 5B. In the similar manner to the preceding sections, $G'(\omega)/\omega^{0.5}$ and $G''(\omega)/\omega^{0.5}$ of untreated HeLa cells (n = 21, red dashed line) and ATP-depleted cells (n = 9, black filled circles) are shown in Fig. 5C and D, respectively. Error bars indicate log-normal SDs. The Mann–Whitney U test for *G'* in the low frequency range (0.1 to 94 Hz) showed significant increase of *G'* upon ATP depletion ($P < 0.05$) compared to the untreated cells.

Feedback-tracking MR in cells can be conducted when the probe particle situates at the homogeneous part of the cell. The experimental errors increases when the probe particle is at the region close to nucleus, cell membranes, or other large organelle, because the inhomogeneity of optical properties in such region disturbs the propagation of the probe and the drive laser. It frequently occurred that a probe particle that was used in the first AMR measurement moves to regions where the measurement is not possible any further. In Fig. S4, we compare the limited numbers of data (n =3) successfully measured using the same probe particle in the same cells. All the results showed the remarkable increase of viscoelasticities when ATP was depleted.

341

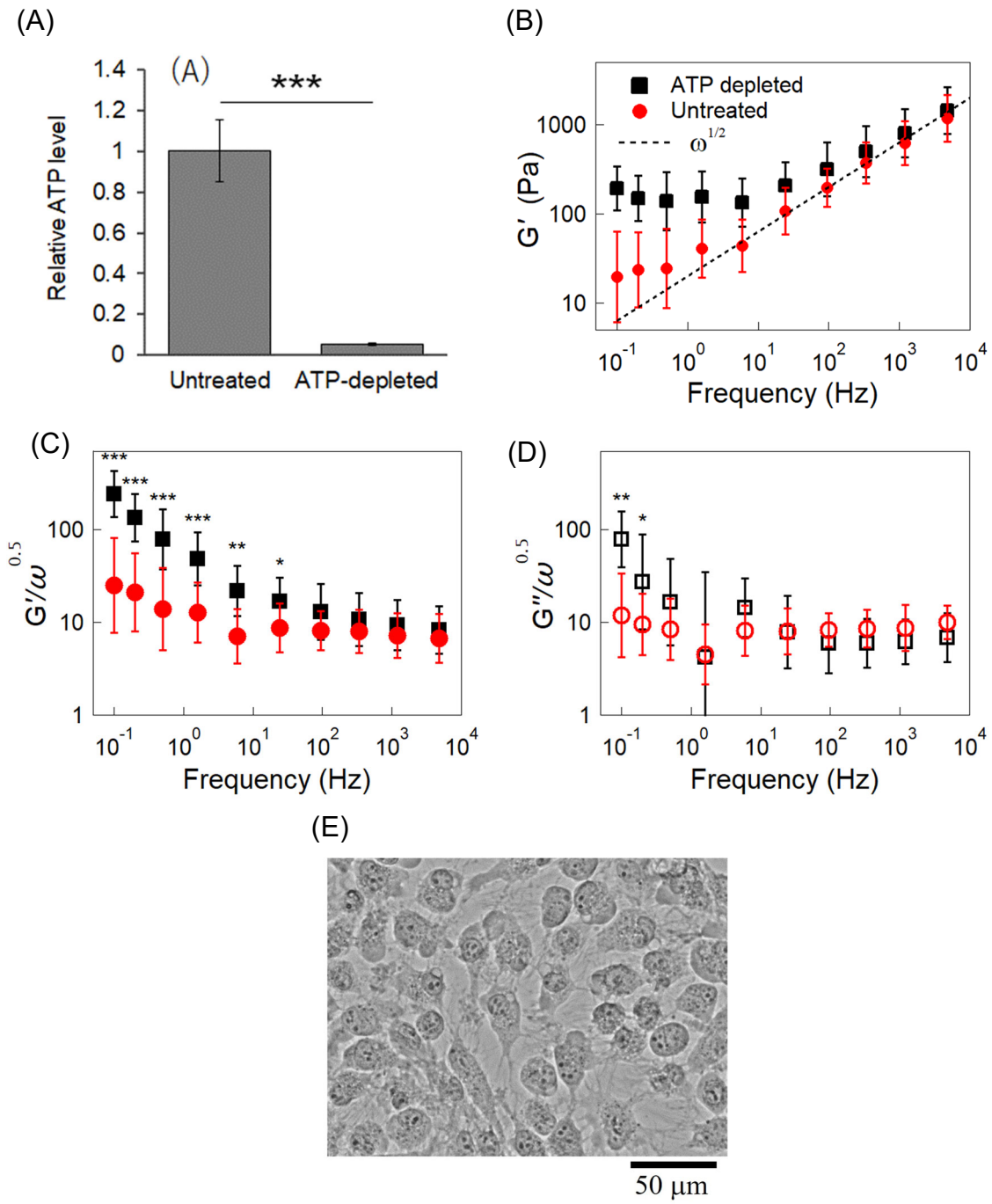

FIGURE 5 (A) Intracellular ATP level in HeLa cells treated with 50 mM 2-deoxyglucose and 10 mM NaN3 (ATP-depleted) for 7 h was measured. Quantification was performed on five independent experiments. All data are presented as mean ± standard deviation. ***: $p < 0.001$ (Student's t-test). (B) $G'(\omega)$ of untreated and ATP-depleted HeLa cells. (C) $G'(\omega)/\omega^{0.5}$ and (D) $G''(\omega)/\omega^{0.5}$ of untreated (red closed circles n = 21) and ATP-depleted HeLa cells (black open squares, n = 9). Bars indicate the log-normal SD. At low frequencies ($f \leq 94$ Hz), $G'(\omega)$ showed significant increase after ATP depletion ($P < 0.05$). (E) Microscope image of ATP-depleted HeLa cells. ATP-depleted HeLa cells became round and lost cell-cell contact. (C, D) The Mann–Whitney U test was used to calculate the P value between untreated and ATP depleted cells. ***: $P < 0.001$. **: $P < 0.01$. *: $P < 0.05$. No symbol: $P > 0.05$.

Figure. 5E shows the microscope images of HeLa cells taken after ATP depletion. ATP-depleted cells lose tight adherence to substrate and to neighboring cells, and change their morphology to more rounded shapes because they decrease cytoskeletal tension. Note that *in vitro* cytoskeletons are remarkably stiffened under active tension or prestress (19, 20, 22). Consistently, the cell surface elasticity measured with AFM decreases when ATP is depleted (64-66) likely because the active stiffening of the cytoskeleton is eased owing to the relax of actomyosin contraction at the cell cortex (57, 67, 68). To the contrary, intracellular elasticity measured in this study increased significantly when the intracellular ATP was depleted. This observation again indicates that the cell cortex cytoskeleton is not relevant to intracellular mechanics. When cells are subjected to the ATP-depletion medium for a prolonged period, they could enter the path towards cell death (69, 70). The fluorescence indicator (fluorescence caspase 3) for the apoptosis indeed showed positive in HeLa cells prepared in the similar protocol (Fig. S5). Except the emergence of the elastic plateau, however, the mechanical properties typical for intracellular rheology $G(\omega) \propto (i\omega)^{0.5}$ were still observed for ATP-depleted cells. Therefore, our results indicate that the cytoplasm with less expression of cytoskeletons stiffens in a metabolism-dependent manner.

DISCUSSION

It has been believed that mechanical properties of cells are mostly determined by cytoskeletons (12, 13). This study showed, however, that the intracellular mechanics in the confluent epithelium are scarce affected by the actin cytoskeletons. Note that there are milliards of other biomacromolecules that are crowded in living cells. Although their effects on cell mechanics have not been fully appreciated until recently, it was shown that *in vitro* cytoplasm that lacks cytoskeletons have glass-forming capabilities; cytoplasm becomes glassy (*i.e.* practically solidified owing to the slowdown of dynamics) when the concentration of polymeric components are increased and/or metabolic activities are inhibited (3, 11, 16, 17, 26). Other prior studies have shown that the spontaneous fluctuations in cells decreased upon ATP depletion (3, 34, 42, 71). It was then inferred that the glassy cytoplasm is fluidized in living cells. However, the decrease/increase of spontaneous fluctuation does not necessarily mean vitrification/fluidization. Even if glass-forming materials are deeply quenched and solidified, they could still flow if they are stirred strongly enough. Besides, only observing the spontaneous fluctuation does not tell us how strongly the medium is stirred by the non-equilibrium activities. In this study, we directly measured the intracellular viscoelasticities by AMR by observing the mechanical response to the well-determined force. Our direct measurement showed that the cytoplasm in ATP-depleted cells was glassy while cells with ordinary metabolic activities were fluidized.

Cells are constructed of soft materials that non-linearly respond to applied forces. For instance, semiflexible polymer networks (cytoskeletons) typically stiffen under tensions (19, 20, 22-24, 72) while glassy suspensions (cytoplasms) are fluidized by mechanical loads (3, 11, 25, 26). In living cells, various mechano-enzymes such as motor proteins perform their

physiological functions by utilizing energy supplied by metabolism. Vigorous fluctuations in living cells do not come from thermal origin, as demonstrated by the violation of the fluctuation-dissipation theorem (10, 73-76). In living cytoplasm, mechano-enzymes drive vigorous fluctuations that surpass the thermal using the energy derived from metabolism (4, 10, 21, 22, 31, 34, 76-81). Owing to the nonlinear response of constituent materials, mechanical properties of cells are altered by the active fluctuations. Here, we again point out that the fluidization of cytoplasm under metabolic activities is consistent to the concept of glassy cytoplasm, but not to cytoskeletons that stiffen with active metabolism (21, 22, 60). Presumably, vigorous active fluctuations induce structural relaxations that could not occur with thermal activations (10, 11), leading to active fluidization.

In accordance with the concept of glassy cytoplasm, mechanical properties in cells showed universal frequency dependency $G(\omega) \propto (-i\omega)^{0.5}$. Recent theoretical studies on jamming rheology have shown that this frequency dependency may be derived from the anomalous relaxation modes existing in the medium at the critical jamming point, crowded with colloidal objects with slippery interfaces (46, 47). When metabolic activity was decreased in ATP-depleted cells, elastic plateau arose as $G(\omega) = G_0 + A(-i\omega)^{0.5}$. Similar viscoelastic behavior with the elastic plateau has been commonly observed in glassy or jammed suspensions which were quenched beyond jamming (47, 82, 83). However, the plateau G_0 seems to disappear when they are driven out of equilibrium under the application of external flow (48), and only $G(\omega) \propto (-i\omega)^{0.5}$ remains in the similar manner with living cytoplasm. Therefore, glassy suspensions may generally exhibit the rheological properties typical for critical jamming [*i.e.*, $G(\omega) \propto (-i\omega)^{0.5}$] when a jammed state is mechanically driven out of equilibrium. Our results in cells may indicate that living cytoplasm is also in such critical situation.

CONCLUSION

In this study, we investigated the mechanical properties of HeLa cells in confluent epithelial monolayer. The probe particle's displacement response to the applied force was observed using the feedback-tracking microrheology technique (10, 24, 33). The shear viscoelastic modulus $G(\omega)$ of cytoplasm surrounding the probe was then obtained. In contrast to prior studies that usually measured the cell's cortex, intracellular shear viscoelastic modulus showed a frequency dependency $G(\omega) \propto (-i\omega)^{0.5}$, which was seldom affected by the cell-cycle progression and the disruption of actin cytoskeletons. On the other hand, the ATP depletion clearly affected the mechanical properties of cell interior; elastic plateau at low frequencies emerged in ATP-depleted cells. These observations are consistent to the recently emerging idea that the cell interior is glassy (3, 11). The activeness of the mechano-enzymes enhances the structural relaxations (yields) as it typically occurs in the glassy medium under mechanical loads. Besides, our results imply that the intracellular cytoplasm is fluidized towards the critical jamming state, characterized by $G(\omega) \propto (-i\omega)^{0.5}$. Although the complete fluidization was not observed in the range of frequencies measured,

the metabolism-dependent glassy mechanics cast various implications. For instance, the positive feedback between mechanics and metabolism may occur in cells because the fluidized cytoplasm could in turn facilitate metabolic processes (3, 8, 11, 71, 84).

ACKNOWLEDGEMENTS

This work was supported by JSPS KAKENHI Grant Number JP22H04848, JP21H01048, JP20H05536, JP20H00128. We thank Christoph Schmidt in Duke University for discussions and technical supports.

CONFLICTS OF INTEREST The authors declare no conflict of interest.

AUTHOR CONTRIBUTION

K.U., K.N., W.N, and H. E. collected and analyzed the MR data. T. M. performed biochemical assays and tests. D. M. designed and supervised the work.

REFERENCES

1. Dix, J. A., and A. S. Verkman. 2008. Crowding effects on diffusion in solutions and cells. Annu Rev Biophys 37:247-263.
2. Minton, A. P. 2001. The influence of macromolecular crowding and macromolecular confinement on biochemical reactions in physiological media. J Biol Chem 276(14):10577-10580.
3. Parry, B. R., I. V. Surovtsev, M. T. Cabeen, C. S. O'Hem, E. R. Dufresne, and C. Jacobs-Wagner. 2014. The Bacterial Cytoplasm Has Glass-like Properties and Is Fluidized by Metabolic Activity. Cell 156(1-2):183-194.
4. Ariga, T., M. Tomishige, and D. Mizuno. 2018. Nonequilibrium Energetics of Molecular Motor Kinesin. Phys Rev Lett 121(21):218101.
5. Ariga, T., K. Tateishi, M. Tomishige, and D. Mizuno. 2021. Noise-Induced Acceleration of Single Molecule Kinesin-1. Phys Rev Lett 127(17):178101.
6. Ezber, Y., V. Belyy, S. Can, and A. Yildiz. 2020. Dynein Harnesses Active Fluctuations of Microtubules for Faster Movement. Nat Phys 16(3):312-316.
7. Riedel, C., R. Gabizon, C. A. Wilson, K. Hamadani, K. Tsekouras, S. Marqusee, S. Presse, and C. Bustamante. 2015. The heat released during catalytic turnover enhances the diffusion of an enzyme. Nature 517(7533):227-230.
8. Jee, A. Y., Y. K. Cho, S. Granick, and T. Tlusty. 2018. Catalytic enzymes are active matter. Proc Natl Acad Sci U S A 115(46):E10812-E10821.
9. Dix, J. A., and A. S. Verkman. 2008. Crowding effects on diffusion in solutions and cells. Annu Rev Biophys 37:247-263.
10. Nishizawa, K., M. Bremerich, H. Ayade, C. F. Schmidt, T. Ariga, and D. Mizuno. 2017. Feedback-tracking microrheology in living cells. Sci Adv 3(9):e1700318.

11. Nishizawa, K., K. Fujiwara, M. Ikenaga, N. Nakajo, M. Yanagisawa, and D. Mizuno. 2017. Universal glass-forming behavior of in vitro and living cytoplasm. Sci Rep 7(1):15143.
12. Fletcher, D. A., and R. D. Mullins. 2010. Cell mechanics and the cytoskeleton. Nature 463(7280):485-492.
13. Rigato, A., A. Miyagi, S. Scheuring, and F. Rico. 2017. High-frequency microrheology reveals cytoskeleton dynamics in living cells. Nat Phys 13(8):771-775.
14. Minton, A. P. 2001. The influence of macromolecular crowding and macromolecular confinement on biochemical reactions in physiological media. J Biol Chem 276(14):10577-10580.
15. Zimmerman, S. B., and S. O. Trach. 1991. Estimation of macromolecule concentrations and excluded volume effects for the cytoplasm of Escherichia coli. J Mol Biol 222(3):599-620.
16. Fabry, B., G. N. Maksym, J. P. Butler, M. Glogauer, D. Navajas, and J. J. Fredberg. 2001. Scaling the microrheology of living cells. Phys Rev Lett 87(14):148102.
17. Zhou, E. H., X. Trepat, C. Y. Park, G. Lenormand, M. N. Oliver, S. M. Mijailovich, C. Hardin, D. A. Weitz, J. P. Butler, and J. J. Fredberg. 2009. Universal behavior of the osmotically compressed cell and its analogy to the colloidal glass transition. Proc Natl Acad Sci U S A 106(26):10632-10637.
18. Fernandez-Marin, B., I. Kranner, M. San Sebastian, U. Artetxe, J. M. Laza, J. L. Vilas, H. W. Pritchard, J. Nadajaran, F. Miguez, J. M. Becerril, and J. I. Garcia-Plazaola. 2013. Evidence for the absence of enzymatic reactions in the glassy state. A case study of xanthophyll cycle pigments in the desiccation-tolerant moss Syntrichia ruralis. J Exp Bot 64(10):3033-3043.
19. Gardel, M. L., J. H. Shin, F. C. MacKintosh, L. Mahadevan, P. Matsudaira, and D. A. Weitz. 2004. Elastic behavior of cross-linked and bundled actin networks. Science 304(5675):1301-1305.
20. Storm, C., J. J. Pastore, F. C. MacKintosh, T. C. Lubensky, and P. A. Janmey. 2005. Nonlinear elasticity in biological gels. Nature 435(7039):191-194.
21. Mizuno, D., C. Tardin, and C. F. Schmidt. 2020. Rapid local compression in active gels is caused by nonlinear network response. Soft Matter 16(40):9369-9382.
22. Mizuno, D., C. Tardin, C. F. Schmidt, and F. C. Mackintosh. 2007. Nonequilibrium mechanics of active cytoskeletal networks. Science 315(5810):370-373.
23. Head, D. A., and D. Mizuno. 2013. Local mechanical response in semiflexible polymer networks subjected to an axisymmetric prestress. Phys Rev E Stat Nonlin Soft Matter Phys 88(2):022717.
24. Honda, N., K. Shiraki, F. Van Esterik, S. Inokuchi, H. Ebata, and D. Mizuno. 2022. Nonlinear master relation in microscopic mechanical response of semiflexible biopolymer networks. New J Phys 24(5).
25. Liu, A. J., and S. R. Nagel. 1998. Jamming is not just cool any more. Nature 396(6706):21-22.
26. Sollich, P., F. Lequeux, P. Hebraud, and M. E. Cates. 1997. Rheology of soft glassy materials. Phys Rev Lett 78(10):2020-2023.

503 27. Nijenhuis, N., D. Mizuno, J. A. Spaan, and C. F. Schmidt. 2012. High-resolution
504 microrheology in the pericellular matrix of prostate cancer cells. J R Soc Interface
505 9(73):1733-1744.
506 28. MacKintosh, F. C., and C. F. Schmidt. 1999. Microrheology. Curr Opin Colloid In
507 4(4):300-307.
508 29. Mason, T. G., K. Ganesan, J. H. vanZanten, D. Wirtz, and S. C. Kuo. 1997. Particle
509 tracking microrheology of complex fluids. Phys Rev Lett 79(17):3282-3285.
510 30. Hough, L. A., and H. D. Ou-Yang. 2002. Correlated motions of two
511 hydrodynamically coupled particles confined in separate quadratic potential wells.
512 Phys Rev E Stat Nonlin Soft Matter Phys 65(2 Pt 1):021906.
513 31. Mizuno, D., D. A. Head, F. C. MacKintosh, and C. F. Schmidt. 2008. Active and
514 Passive Microrheology in Equilibrium and Nonequilibrium Systems.
515 Macromolecules 41(19):7194-7202.
516 32. Gittes, F., and C. F. Schmidt. 1998. Interference model for back-focal-plane
517 displacement detection in optical tweezers. Opt Lett 23(1):7-9.
518 33. Sugino, Y., M. Ikenaga, and D. Mizuno. 2020. Optimization of Optical Trapping and
519 Laser Interferometry in Biological Cells. Appl Sci-Basel 10(14).
520 34. Guo, M., A. J. Ehrlicher, M. H. Jensen, M. Renz, J. R. Moore, R. D. Goldman, J.
521 Lippincott-Schwartz, F. C. Mackintosh, and D. A. Weitz. 2014. Probing the
522 Stochastic, Motor-Driven Properties of the Cytoplasm Using Force Spectrum
523 Microscopy. Cell 158(4):822-832.
524 35. Alberts, B. 2015. Molecular biology of the cell. Garland Science, Taylor and Francis
525 Group, New York, NY.
526 36. Yusko, E. C., and C. L. Asbury. 2014. Force is a signal that cells cannot ignore. Mol
527 Biol Cell 25(23):3717-3725.
528 37. Huang, S., C. S. Chen, and D. E. Ingber. 1998. Control of cyclin D1, p27(Kip1), and
529 cell cycle progression in human capillary endothelial cells by cell shape and
530 cytoskeletal tension. Mol Biol Cell 9(11):3179-3193.
531 38. Klein, E. A., L. Yin, D. Kothapalli, P. Castagnino, F. J. Byfield, T. Xu, I. Levental,
532 E. Hawthorne, P. A. Janmey, and R. K. Assoian. 2009. Cell-cycle control by
533 physiological matrix elasticity and in vivo tissue stiffening. Curr Biol 19(18):1511-
534 1518.
535 39. Kelly, G. M., J. I. Kilpatrick, M. H. van Es, P. P. Weafer, P. J. Prendergast, and S. P.
536 Jarvis. 2011. Bone cell elasticity and morphology changes during the cell cycle. J
537 Biomech 44(8):1484-1490.
538 40. Tsai, M. A., R. E. Waugh, and P. C. Keng. 1996. Cell cycle-dependence of HL-60
539 cell deformability. Biophys J 70(4):2023-2029.
540 41. Haga, H., S. Sasaki, K. Kawabata, E. Ito, T. Ushiki, and T. Sambongi. 2000. Elasticity
541 mapping of living fibroblasts by AFM and immunofluorescence observation of the
542 cytoskeleton. Ultramicroscopy 82(1-4):253-258.
543 42. Hoffman, B. D., G. Massiera, K. M. Van Citters, and J. C. Crocker. 2006. The
544 consensus mechanics of cultured mammalian cells. Proc Natl Acad Sci U S A
545 103(27):10259-10264.

43. Fabry, B., G. N. Maksym, J. P. Butler, M. Glogauer, D. Navajas, N. A. Taback, E. J. Millet, and J. J. Fredberg. 2003. Time scale and other invariants of integrative mechanical behavior in living cells. Phys Rev E Stat Nonlin Soft Matter Phys 68(4 Pt 1):041914.
44. Gittes, F., and F. C. MacKintosh. 1998. Dynamic shear modulus of a semiflexible polymer network. Phys Rev E 58(2):R1241-R1244.
45. Koenderink, G. H., M. Atakhorrami, F. C. MacKintosh, and C. F. Schmidt. 2006. High-frequency stress relaxation in semiflexible polymer solutions and networks. Phys Rev Lett 96(13):138307.
46. Tighe, B. P. 2011. Relaxations and rheology near jamming. Phys Rev Lett 107(15):158303.
47. Liu, A. J., S. Ramaswamy, T. G. Mason, H. Gang, and D. A. Weitz. 1996. Anomalous viscous loss in emulsions. Phys Rev Lett 76(16):3017-3020.
48. Jacob, A. R., A. S. Poulos, A. N. Semenov, J. Vermant, and G. Petekidis. 2019. Flow dynamics of concentrated starlike micelles: A superposition rheometry investigation into relaxation mechanisms. J Rheol 63(4):641-653.
49. He, J., and J. X. Tang. 2011. Surface adsorption and hopping cause probe-size-dependent microrheology of actin networks. Phys Rev E Stat Nonlin Soft Matter Phys 83(4 Pt 1):041902.
50. Koenderink, G. H., M. Atakhorrami, F. C. MacKintosh, and C. F. Schmidt. 2006. High-frequency stress relaxation in semiflexible polymer solutions and networks. Phys Rev Lett 96(13).
51. Morse, D. C. 1998. Viscoelasticity of concentrated isotropic solutions of semiflexible polymers. 2. Linear response. Macromolecules 31(20):7044-7067.
52. Morse, D. C. 1998. Viscoelasticity of concentrated isotropic solutions of semiflexible polymers. 1. Model and stress tensor. Macromolecules 31(20):7030-7043.
53. Caspi, A., M. Elbaum, R. Granek, A. Lachish, and D. Zbaida. 1998. Semiflexible polymer network: A view from inside. Phys Rev Lett 80(5):1106-1109.
54. Casella, J. F., M. D. Flanagan, and S. Lin. 1981. Cytochalasin D inhibits actin polymerization and induces depolymerization of actin filaments formed during platelet shape change. Nature 293(5830):302-305.
55. Wakatsuki, T., B. Schwab, N. C. Thompson, and E. L. Elson. 2001. Effects of cytochalasin D and latrunculin B on mechanical properties of cells. J Cell Sci 114(Pt 5):1025-1036.
56. Wang, A., K. Vijayraghavan, O. Solgaard, and M. J. Butte. 2016. Fast Stiffness Mapping of Cells Using High-Bandwidth Atomic Force Microscopy. Acs Nano 10(1):257-264.
57. Bacabac, R. G., D. Mizuno, C. F. Schmidt, F. C. MacKintosh, J. J. W. A. Van Loon, J. Klein-Nulend, and T. H. Smit. 2007. ROUND VERSUS FLAT: BONE CELL MORPHOLOGY, ELASTICITY, AND MECHANOSENSING J Biomech.
58. Stewart, M. P., J. Helenius, Y. Toyoda, S. P. Ramanathan, D. J. Muller, and A. A. Hyman. 2011. Hydrostatic pressure and the actomyosin cortex drive mitotic cell rounding. Nature 469(7329):226-230.

59. Rotsch, C., and M. Radmacher. 2000. Drug-induced changes of cytoskeletal structure and mechanics in fibroblasts: an atomic force microscopy study. Biophys J 78(1):520-535.
60. Koenderink, G. H., Z. Dogic, F. Nakamura, P. M. Bendix, F. C. MacKintosh, J. H. Hartwig, T. P. Stossel, and D. A. Weitz. 2009. An active biopolymer network controlled by molecular motors. Proc Natl Acad Sci U S A 106(36):15192-15197.
61. Sakaue-Sawano, A., H. Kurokawa, T. Morimura, A. Hanyu, H. Hama, H. Osawa, S. Kashiwagi, K. Fukami, T. Miyata, H. Miyoshi, T. Imamura, M. Ogawa, H. Masai, and A. Miyawaki. 2008. Visualizing spatiotemporal dynamics of multicellular cell-cycle progression. Cell 132(3):487-498.
62. Taubenberger, A. V., B. Baum, and H. K. Matthews. 2020. The Mechanics of Mitotic Cell Rounding. Front Cell Dev Biol 8:687.
63. Hurst, S., B. E. Vos, M. Brandt, and T. Betz. 2021. Intracellular softening and increased viscoelastic fluidity during division. Nat Phys 17(11):1270-+.
64. Gupta, S. K., and M. Guo. 2017. Equilibrium and out-of-equilibrium mechanics of living mammalian cytoplasm. J Mech Phys Solids 107:284-293.
65. Streppa, L., F. Ratti, E. Goillot, A. Devin, L. Schaeffer, A. Arneodo, and F. Argoul. 2018. Prestressed cells are prone to cytoskeleton failures under localized shear strain: an experimental demonstration on muscle precursor cells. Sci Rep 8(1):8602.
66. Embry, A. E., H. Mohammadi, X. Niu, L. Liu, B. Moe, W. A. Miller-Little, C. Y. Lu, L. A. Bruggeman, C. A. McCulloch, P. A. Janmey, and R. T. Miller. 2016. Biochemical and Cellular Determinants of Renal Glomerular Elasticity. Plos One 11(12):e0167924.
67. Sutton, T. A., H. E. Mang, and S. J. Atkinson. 2001. Rho-kinase regulates myosin II activation in MDCK cells during recovery after ATP depletion. Am J Physiol-Renal 281(5):F810-F818.
68. Yubero, M. L., P. M. Kosaka, A. San Paulo, M. Malumbres, M. Calleja, and J. Tamayo. 2020. Effects of energy metabolism on the mechanical properties of breast cancer cells. Commun Biol 3(1).
69. Eguchi, Y., S. Shimizu, and Y. Tsujimoto. 1997. Intracellular ATP levels determine cell death fate by apoptosis or necrosis. Cancer Res 57(10):1835-1840.
70. Lieberthal, W., S. A. Menza, and J. S. Levine. 1998. Graded ATP depletion can cause necrosis or apoptosis of cultured mouse proximal tubular cells. Am J Physiol 274(2):F315-327.
71. Weber, S. C., A. J. Spakowitz, and J. A. Theriot. 2012. Nonthermal ATP-dependent fluctuations contribute to the in vivo motion of chromosomal loci. Proc Natl Acad Sci U S A 109(19):7338-7343.
72. Head, D. A., E. Ikebe, A. Nakamasu, P. Zhang, L. G. Villaruz, S. Kinoshita, S. Ando, and D. Mizuno. 2014. High-frequency affine mechanics and nonaffine relaxation in a model cytoskeleton. Phys Rev E Stat Nonlin Soft Matter Phys 89(4):042711.
73. Umeda, K., K. Nishizawa, W. Nagao, Y. Sugino, N. Oyama, H. Ebata, and D. Mizuno. To be submitted. Activity-dependent glassy mechanics in living cells II; Non-thermal fluctuations under metabolic activity.

632 74. Mizuno, D., C. Tardin, C. F. Schmidt, and F. C. MacKintosh. 2007. Nonequilibrium
633 mechanics of active cytoskeletal networks. Science 315(5810):370-373.
634 75. Ahmed, W. W., E. Fodor, M. Almonacid, M. Bussonnier, M. H. Verlhac, N. Gov, P.
635 Visco, F. van Wijland, and T. Betz. 2018. Active Mechanics Reveal Molecular-Scale
636 Force Kinetics in Living Oocytes. Biophysical Journal 114(7):1667-1679.
637 76. Turlier, H., D. A. Fedosov, B. Audoly, T. Auth, N. S. Gov, C. Sykes, J. F. Joanny, G.
638 Gompper, and T. Betz. 2016. Equilibrium physics breakdown reveals the active
639 nature of red blood cell flickering. Nat Phys 12(5):513-+.
640 77. Mizuno, D., R. Bacabac, C. Tardin, D. Head, and C. F. Schmidt. 2009. High-
641 resolution probing of cellular force transmission. Phys Rev Lett 102(16):168102.
642 78. Harada, T., and S. Sasa. 2005. Equality connecting energy dissipation with a violation
643 of the fluctuation-response relation. Phys Rev Lett 95(13):130602.
644 79. Lau, A. W., B. D. Hoffman, A. Davies, J. C. Crocker, and T. C. Lubensky. 2003.
645 Microrheology, stress fluctuations, and active behavior of living cells. Phys Rev Lett
646 91(19):198101.
647 80. Bertrand, O. J., D. K. Fygenson, and O. A. Saleh. 2012. Active, motor-driven
648 mechanics in a DNA gel. Proc Natl Acad Sci U S A 109(43):17342-17347.
649 81. Ahmed, W. W., E. Fodor, M. Almonacid, M. Bussonnier, M. H. Verlhac, N. Gov, P.
650 Visco, F. van Wijland, and T. Betz. 2018. Active Mechanics Reveal Molecular-Scale
651 Force Kinetics in Living Oocytes. Biophys J 114(7):1667-1679.
652 82. Wyss, H. M., K. Miyazaki, J. Mattsson, Z. Hu, D. R. Reichman, and D. A. Weitz.
653 2007. Strain-rate frequency superposition: a rheological probe of structural relaxation
654 in soft materials. Phys Rev Lett 98(23):238303.
655 83. Krishan, K., A. Helal, R. Hohler, and S. Cohen-Addad. 2010. Fast relaxations in foam.
656 Phys Rev E Stat Nonlin Soft Matter Phys 82(1 Pt 1):011405.
657 84. Ross, J. L. 2016. The Dark Matter of Biology. Biophys J 111(5):909-916.
658